RSC Advances

PAPER

View Article Online
View Journal | View Issue

Cite this: *RSC Adv.*, 2021, **11**, 13521

Mesoporous adsorbent for competitive adsorption of fluoride ions in zinc sulfate solution

Lisi Liang, Jiayu Mi, Linbo Li, * Xihong He and Wenlong Guo

Al–La hybrid gel was constructed using an innovative acid-catalyzed and calcination free sol–gel formation process which only included a sol–gel process lasting for 30 min and a drying procedure at 150 °C. This novel material was used as an adsorbent for competitive adsorption of fluoride ions in zinc sulfate solution. The properties, optimal adsorption conditions, synthetic principle and adsorption mechanism of the material were systemically investigated. The results showed that γ-AlO(OH) composed the skeleton of the Al–La hybrid gel and $La(CH_3COO)_3$ was embedded in the framework, which formed large amounts of ink-bottle type mesopores. A high fluoride ion adsorption rate with the removal rate reaching 50.88% within 1 min at 50 °C, 3 g L^{-1} was obtained. Analysis of the adsorption data has demonstrated that the adsorption of fluoride ions by the Al–La hybrid gel followed pseudo-second-order kinetics. Moreover, both Langmuir and Freundlich models can describe the adsorption process well. The maximum adsorption capacity of the Al–La hybrid adsorbent was 28.383 mg g^{-1}. Furthermore, the mechanism analysis results indicated that the fluoride ions were mainly removed by the electrostatic adsorption on the AlO(OH), and a small amount of fluoride ions was also adsorbed by the complexation of lanthanum and fluoride ions. Since both AlO(OH) and $La(CH_3COO)_3$ had a large number of fluoride ion adsorption sites, the Al–La hybrid gel obtained an ideal adsorption capacity. In addition, the adsorption rate was greatly enhanced by the capillary action existing from the initial to the final stage of adsorption.

Received 30th January 2021
Accepted 31st March 2021

DOI: 10.1039/d1ra00802a

rsc.li/rsc-advances

1. Introduction

Fluoride ions often cause adverse effects on industrial production and the environment.[1–4] Currently, over 80% of zinc is produced through a hydrometallurgy process which is regarded as more eco-friendly.[5,6] In the aforementioned practice, high concentrations of fluoride ions can cause multiple problems. Fluoride ions corrode the oxide film on the surface of the aluminum plate during the electrolytic deposition stage, which makes the cathode aluminum plate and the precipitated zinc bond together, increasing the difficulty of zinc stripping and consumption of the aluminum plate. Besides that, the corrosion of fluoride ions on the anode plate shortens the service time of the anode, and the presence of large amounts of fluoride ions with high toxicity worsens the working environment.[7,8] Therefore, the realization of efficient defluoridation from zinc sulfate solution is significant. In numerous defluoridation technologies, adsorption has received extensive attention for high efficiency and low cost.[9–11] Aluminum-based adsorbents are the most widely used fluoride ion sorbents with exceptional adsorption effects and low prices.[12–14] However, the adsorption capacity and speed of traditional aluminum adsorbents are relatively low, so they need to be modified to get better adsorption properties. Rare earth compounds have a large adsorption capacity, low toxicity, and high selectivity to fluoride ions, but are expensive because of scarcity.[15–18] Therefore, it is considered meaningful to modify aluminum sorbents with rare earth elements, which could combine the advantages of both materials.

There has been some progress in the research of rare earth modified aluminum-based materials used as fluoride ion adsorbents. Cheng *et al.* synthesized alumina (La-AA) adsorbent through dipping method which included a procedure of mixing reagents for two days.[12] Wei *et al.* prepared Ca–Al–La composite sorbent by a one-step hydrothermal process which included an 8 h high temperature and pressure heating technique.[19] However, the previous studies were aimed at the removal of fluoride ions in aqueous solutions rather than zinc sulfate electrolytes with much more complicated solution composition and ions form. In addition, the simpler preparation processing of this kind of adsorbent needs to be explored to reduce the consumption of time and energy.

In this study, Al–La hybrid gel prepared by innovative sol–gel method were used as fluoride ion sorbent. This method only included a rapid sol–gel processing lasting for 30 min and a drying procedure at 150 °C, which eliminated the high-temperature roasting process of typical sol–gel technique and quite differed from other preparation technologies with long

School of Metallurgical Engineering, Xi'an University of Architecture and Technology, Xi'an 710055, China. E-mail: 13152158058@163.com

Table 1 Main ingredients of the simulated zinc sulfate solution

Composition	Zn	Cu	Cl	F
Concentration (g L^{-1})	130	0.2	0.36	0.07

flow or large time consuming. The material was used to adsorb fluoride ions in zinc sulfate solution and has been evaluated under different conditions including the amount of adsorbent, adsorption temperature and contact time. The properties of gel were characterized *via* using a variety of techniques, and the adsorption kinetics and isotherms were investigated. Additionally, the synthetic principle and adsorption mechanism of the adsorbent were explored.

2. Experimental

2.1. Chemicals

Pseudo-boehmite was the type of high purity and low sodium, which was purchased from Jinghuo Company (Shandong, China). Other reagents ($La(NO_3)_3 \cdot 6H_2O$, $C_2H_4O_2$, $ZnSO_4 \cdot 7H_2O$, $CuSO_4 \cdot 5H_2O$, NaF, NaCl) were analytical grade. The simulated zinc sulfate solution was prepared referring to the actual solution composition of a smelter. 56.169 g $ZnSO_4 \cdot 7H_2O$, 0.0785 g $CuSO_4 \cdot 5H_2O$, 0.0329 g NaCl and 0.0221 g NaF were weighed and dissolved in 80 mL deionized water, preparing 100 mL simulated zinc sulfate solution. The main elemental contents of the solution are listed in Table 1.

2.2. Preparation

The Al–La hybrid adsorbent was prepared by acid-catalyzed and calcination free sol–gel method: 0.374 g $La(NO_3)_3 \cdot 6H_2O$ was weighed and dissolved in deionized water. After the solute dissolved, 1.621 g pseudo-boehmite was added into the solution under stirring. Until the mixing procedure continued for 30 min, the acetic acid solution was added to turn the turbid liquid into a sol. Finally, powdery dry gel was obtained through low-temperature drying (150 °C) and grinding steps. Schematic diagram of Al–La hybrid adsorbent preparation is displayed as Fig. 1.

2.3. Characterization

The phase of the adsorbent was confirmed by X-ray diffraction (XRD, X′ Pert PRO) with Cu Kα radiation, the test conditions were: scanning angle range 5–90°, scanning speed 5 (°) min^{-1}, accelerating voltage 45 kV, applied current 40 mA. The morphology of the material was tested by Scanning Electron Microscope (SEM, SU8220) and Transmission Electron Microscope (TEM, FEI Talos-S). The specific surface area and pore size distribution of the adsorbent were measured by BET analysis (ASAP2460).

2.4. Batch experiments

15 mL simulated zinc sulfate solution was added to 25 mL centrifuge tube. The calculated amount of powdered gel was added into the centrifuge tube. And the mixture was shaken in

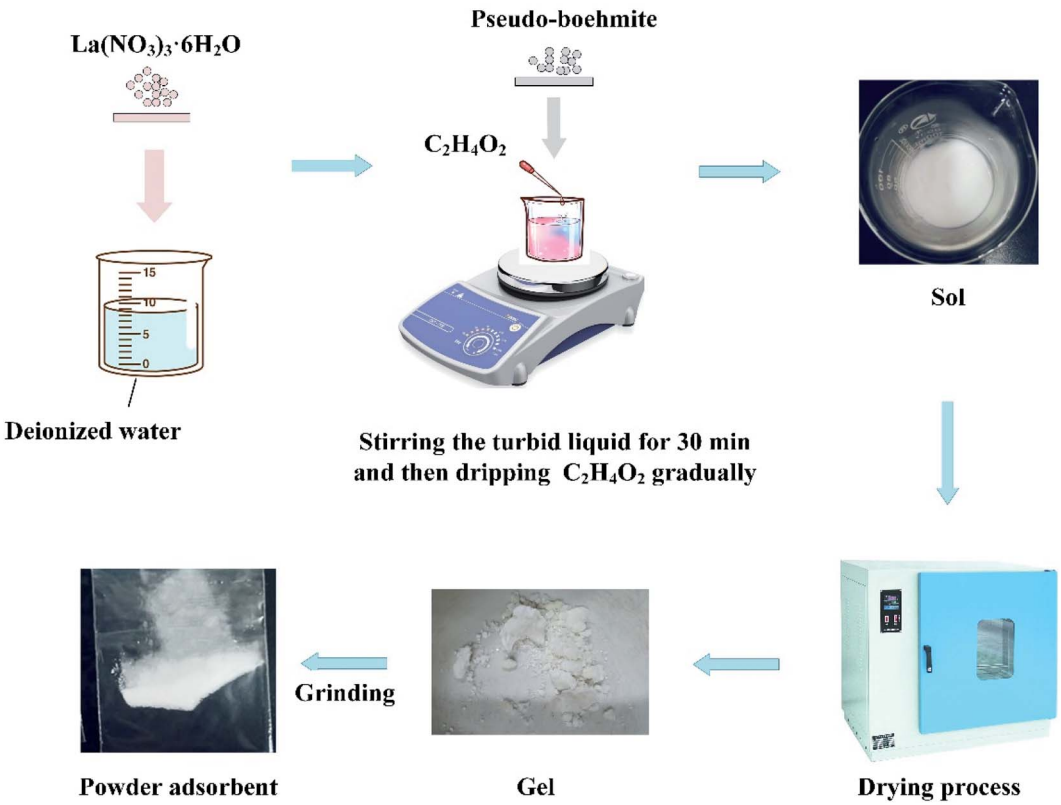

Fig. 1 Schematic diagram of innovative sol–gel method.

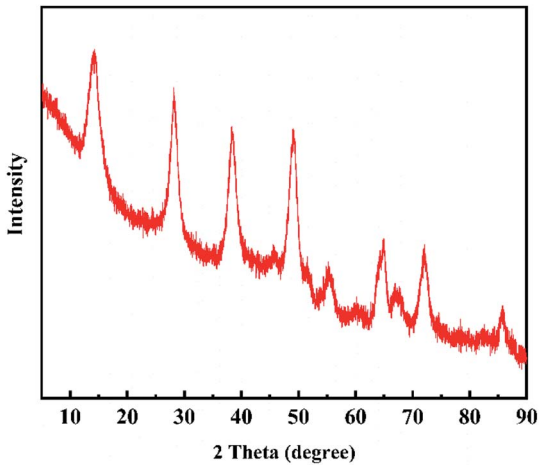

Fig. 2 XRD pattern of the Al–La hybrid adsorbent.

a reciprocating constant temperature water bath oscillator at 120 rpm within a certain contact time. After adsorption, adsorbent and zinc sulfate solution were separated by filtration. The concentration of fluoride ions in solution before and after adsorption were measured by the fluoride ion selective electrode (BPX-932, Bell, China), and the defluoridation performance of the adsorbent was assessed by the calculation of eqn (1).

$$q_e = (C_0 - C_e)V/m \quad (1)$$

where q_e is the adsorption capacity of fluoride ions per unit weight of adsorbent (mg g^{-1}) at equilibrium, C_0 is the initial fluoride concentration (mg L^{-1}), C_e is the equilibrium fluoride concentration (mg L^{-1}), V is the volume (mL) of the zinc sulfate solution and m is the amount of adsorbent (g).

To further explore the optimal conditions for adsorption, the experiments based on variable factors were operated. To study the effect of adsorption temperature, the adsorption temperatures were controlled from 30 to 70 °C, respectively. The adsorbent dose was 10 g L^{-1} and the contact time was limited to 65 min. In the investigation of the effect of amount of adsorbent, the doses were adjusted to 1 g L^{-1}, 3 g L^{-1}, 5 g L^{-1}, 10 g L^{-1} or 15 g L^{-1}. The adsorption temperature was 50 °C and the contact time was controlled under 65 min.

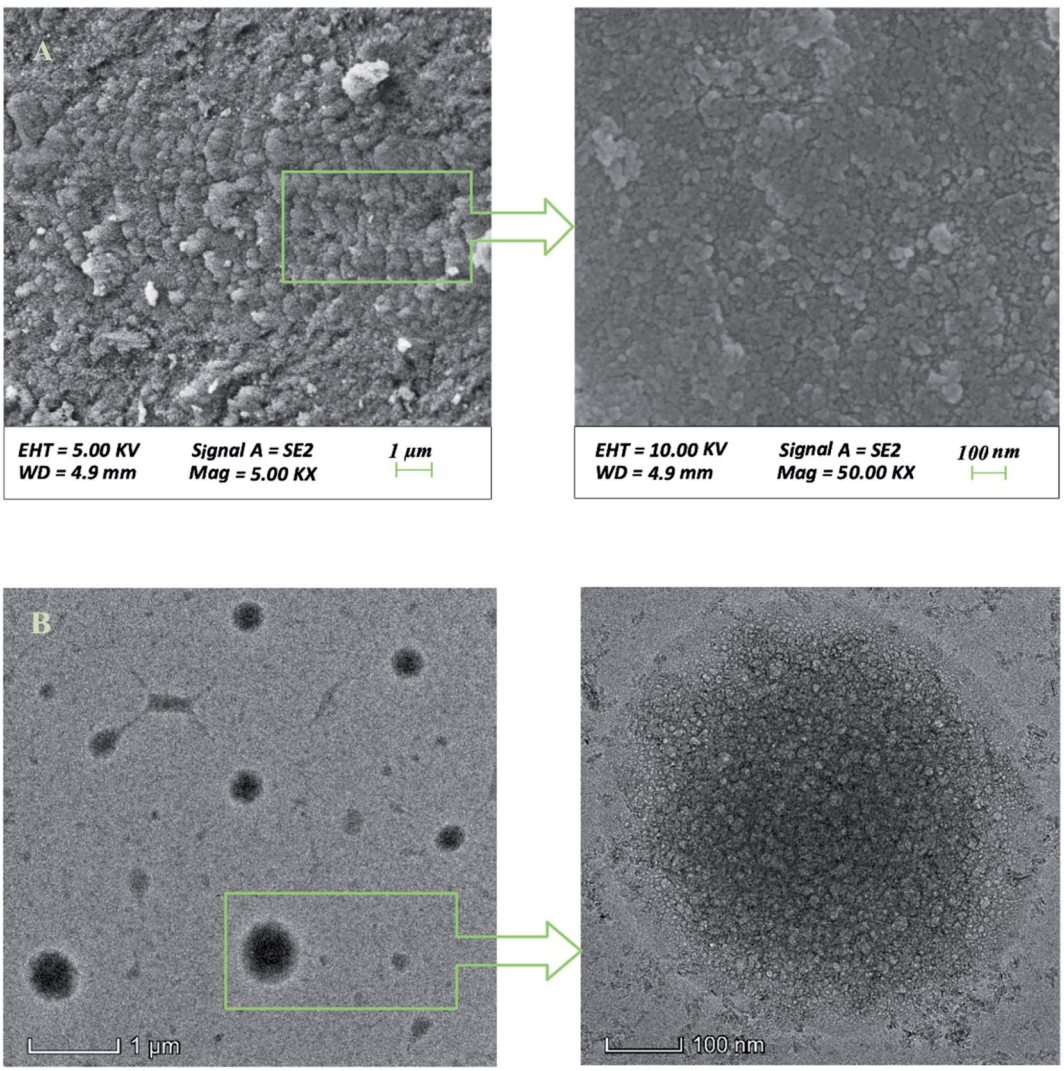

Fig. 3 SEM images (A) and TEM images (B) of the Al–La hybrid adsorbent.

To study the kinetic on the adsorption process, the fluoride ion content was measured in different time points from 1 to 64 min. The adsorption temperature was 50 °C and the adsorbent dose was 3 g L^{-1}.

To obtain the adsorption isotherm on the process, simulated solutions with initial fluoride ion concentrations from 10 to 250 mg L^{-1} were prepared. The adsorption temperature was 50 °C; the adsorbent dose was 3 g L^{-1} and the contact time was 64 min.

3. Results and discussion

3.1. Characterization results

3.1.1. XRD pattern. The XRD pattern of the Al–La hybrid sample is exhibited in Fig. 2. It could be seen that most of the diffraction peaks were the characteristic peaks of γ-AlO(OH), especially those at $2\theta = 13.9990°$, 28.2015°, 38.3883°, 49.3223°. Thus, the principal phase of the sample was γ-AlO(OH).

3.1.2. Electron microscope images. The SEM images of the as-prepared sample are showed in Fig. 3A. It could be observed that the sample had a relatively rough surface. The TEM images of the adsorbent (Fig. 3B) show that the host phase with low crystallinity was of a similar structure to the traditional γ-AlO(OH), confirming that the host phase of the gel was γ-AlO(OH). The lanthanum complex loaded on hydroxy alumina had fine crystallinity, and the areas where the compound was concentrated contained a large number of mesopores.

3.1.3. BET analysis. The N_2 adsorption–desorption isotherms of the Al–La hybrid gel is displayed in Fig. 4. According to the classification of IUPAC,[20] the isotherm linear plot of hybrid adsorbent could be classified as type IV isotherms type-H_2 hysteresis loop, which indicated the mesoporous nature of synthesized materials. At lower pressures, the adsorption capacity increased slowly. H_2 hysteresis loop were presented with the increase of relative pressures, revealing the presence of pores with narrow neck and wide body (often in the form of ink bottle pores).[21] The pore distributed plot (Fig. 4B) reflected the average pore size of 3.358 nm, confirming the existence of mesopores. In addition, the specific surface area of the material was measured as 183.537 m^2 g^{-1}. The decrease in surface area can be attributed to the filling of rare earth compound on hydroxy alumina.[22,23]

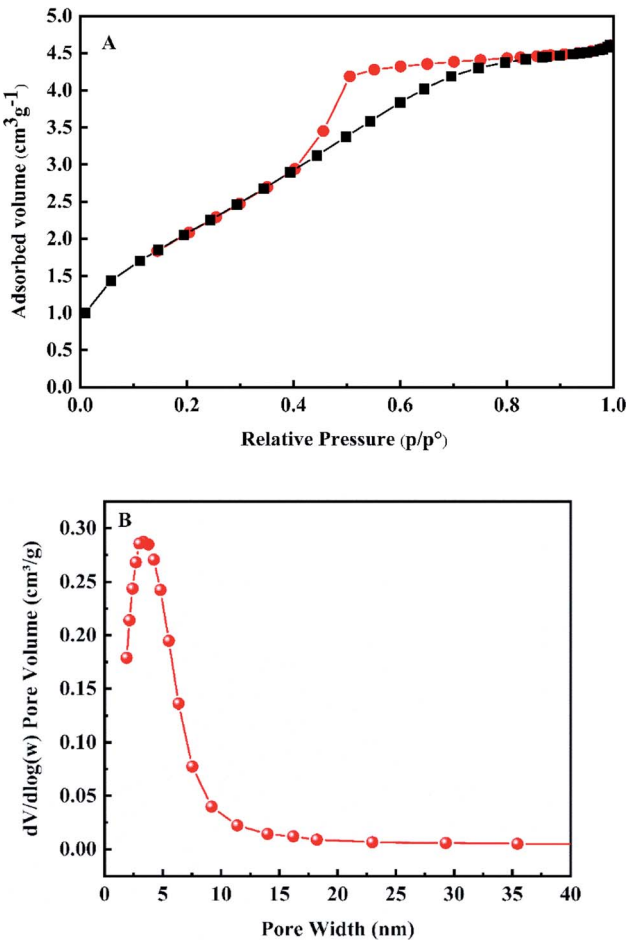

Fig. 4 N_2 adsorption–desorption isotherms (A) and BJH pore size distribution curve (B) of the Al–La hybrid adsorbent.

3.2. Optimization of application conditions

The effect of adsorption temperature on adsorbed capacity of the material is shown in Fig. 5. It could be observed that the adsorption capacity increased firstly and then decreased with the adsorption temperature from 30 °C to 70 °C, and the best adsorption efficiency could be obtained at 50 °C. Therefore, the temperature of the adsorption process was designated as 50 °C.

The effect of the amount of adsorbent on defluoridation ability of the material is depicted in Fig. 6. It was found that when the amount of adsorbent from 1 g L^{-1} to 3 g L^{-1}, the concentrations of residual fluoride ions decreased from 46.110 mg L^{-1} to 22.425 mg L^{-1} rapidly. As the amount of adsorbent increased from 3 g L^{-1} to 10 g L^{-1}, the decrease in the fluoride ion equilibrium concentration was greatly reduced. When the amount of adsorbent was further increased to 15 g L^{-1}, the residual fluoride ion concentration showed an upward trend unexpectedly, which may be due to the flocculation

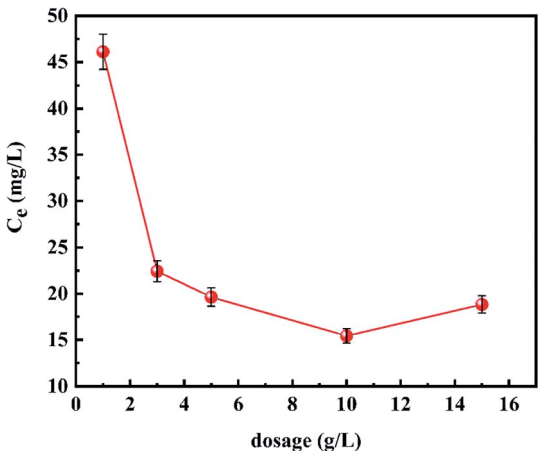

Fig. 5 Effect of adsorption temperature (where q_e (mg g^{-1}) is the equilibrium adsorption capacity of the material, amount of adsorbent: 10 g L^{-1}, initial fluoride ion concentration: 70.0 mg L^{-1}, contact time: 65 min, pH: 4.5).

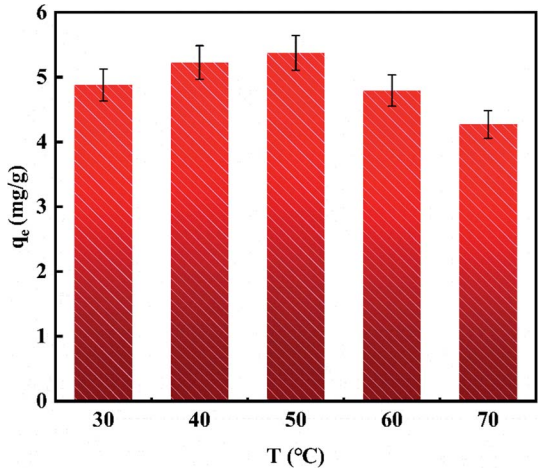

Fig. 6 Effect of amount of adsorbent (where C_e (mg L^{-1}) is the equilibrium concentration of fluoride ions, temperature: 50 °C, initial fluoride ion concentration: 70.0 mg L^{-1}, contact time: 65 min, pH: 4.5).

phenomenon in the case of excessive powdered adsorbent. Thus, 3 g L^{-1} was selected as the optimal amount of adsorbent.

The effect of the contact time of the adsorption process is presented in Fig. 7. It was obvious that the concentration of remaining fluoride ions in the solution dropped sharply from 32.934 mg L^{-1} to 23.857 mg L^{-1} in the first 16 min, then the downward trend became slow. Eventually, fluoride ion equilibrium concentration in the simulated solution remained unchanged at 20.685 mg L^{-1} after 64 min. Therefore, it can be considered that when the adsorption temperature and amount of adsorbent were 50 °C and 3 g L^{-1} respectively, the adsorption equilibrium time after modification was shortened to 64 min. Besides, the high fluoride ions adsorption rate with the removal rate reaching 50.88% within 1 min at 50 °C, 3 g L^{-1} was obtained.

3.3. Adsorption kinetics

To further evaluate the adsorption kinetics, the above data was further analyzed by kinetic equations including the pseudo-first-order and pseudo-second-order models.[24–27]

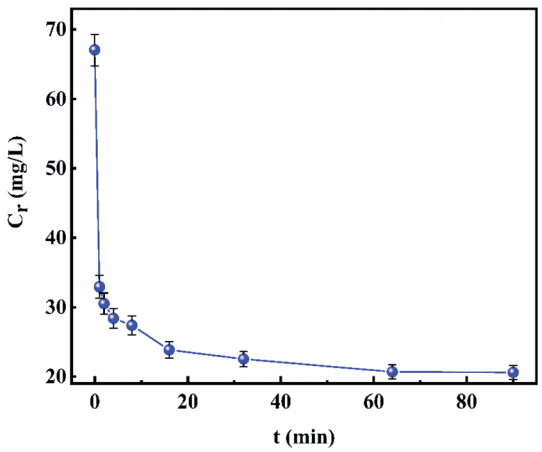

Fig. 7 Effect of contact time (where C_r (mg L^{-1}) is the residual concentration of fluoride ions, temperature: 50 °C, initial fluoride ion concentration: 70.0 mg L^{-1}, amount of adsorbent: 3 g L^{-1}, pH: 4.5).

The pseudo-first-order rate equation can be given as eqn (2).

$$\ln(q_e - q_t) = \ln q_e - k_1 t \quad (2)$$

The pseudo-second-order rate equation is expressed as eqn (3).

$$t/q_t = 1/k_2 q_e^2 + t/q_e \quad (3)$$

where q_e (mg g^{-1}) and q_t (mg g^{-1}) are the adsorbed capacities of fluoride ions on the Al–La hybrid adsorbent at equilibrium and at time t respectively. k_1 and k_2 are the rate constants of the pseudo-first-order and pseudo-second-order models. The value of q_e, k_1 and k_2 could be obtained from the fitting plots (Fig. 8) and are shown in Table 2.

As shown in Table 2, the goodness of fit of the pseudo-second-order model was better than that of the pseudo-first-order model with the correlation coefficient (R^2) 0.99954 and 0.94766, respectively. In addition, the $q_{e,cal}$ value from the pseudo-second-order (15.373 mg g^{-1}) was closed to the experimental value (15.460 mg g^{-1}). Therefore, the pseudo-second-order kinetic model can explain the adsorption process well,

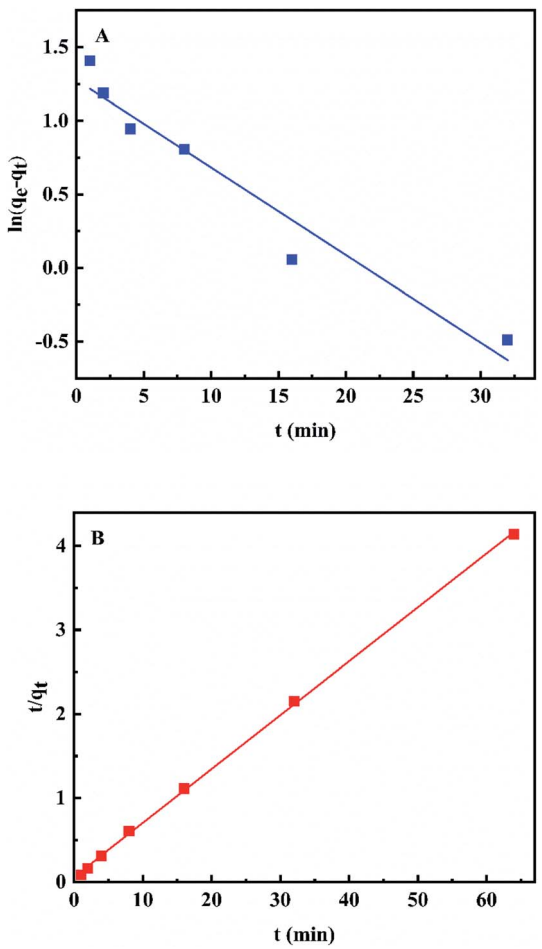

Fig. 8 Pseudo-first-order (A) and pseudo-second-order (B) kinetic model fitting plots for fluoride ion adsorption on the Al–La hybrid adsorbent.

Table 2 Kinetic parameters for fluoride ion adsorption on the Al–La hybrid adsorbent

	Pseudo-first-order model			Pseudo-second-order model		
$q_{e.exp}$ (mg g^{-1})	K_1 (min^{-1})	$q_{e.cal}$ (mg g^{-1})	R^2	K_2 [g (min^{-1} g^{-1})]	$q_{e.cal}$ (mg g^{-1})	R^2
15.460	0.05949	15.354	0.94766	0.06419	15.373	0.99954

indicating that the rate-limiting step was the surface adsorption involving chemisorption.[28] The high rate constant k_2 of Al–La hybrid adsorbent indicated the fast adsorption kinetics of fluoride ions on Al–La hybrid adsorbent. Meanwhile, the initial adsorption rate of gel was 11.372 mg g^{-1} min^{-1}.

3.4. Adsorption isotherms

To further explore the adsorption mechanism, the adsorption isotherm was investigated. In recent research, Langmuir and Freundlich adsorption isotherm models are usually used to describe the adsorption isotherms.[29–34]

The Langmuir isotherm model describes the monolayer adsorption process in an ideal uniform sorption state. The primitive equation of the Langmuir model is given as eqn (4).

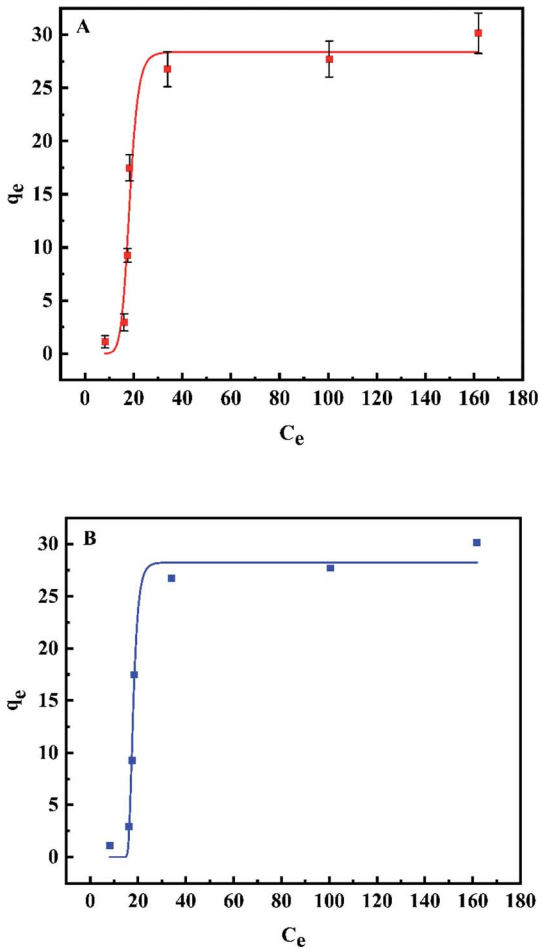

Fig. 9 Fitting plots of the Langmuir adsorption isotherm (A) and Freundlich adsorption isotherm (B). (Temperature: 50 °C, amount of adsorbent: 3 g L^{-1}, contact time: 64 min, pH: 4.5).

$$q_e = q_m \frac{K_L C_e}{1 + K_L C_e} \quad (4)$$

where q_e (mg g^{-1}) is the equilibrium adsorption capacity of the material, C_e (mg L^{-1}) is the equilibrium concentration of fluoride ions, q_m (mg g^{-1}) is the maximum adsorption capacity and K_L (L mg^{-1}) is the Langmuir constant.

The Freundlich isotherm model describes the multi-layer adsorption process in a heterogeneous adsorption state. The primitive equation of the Freundlich model is expressed as eqn (5).

$$q_e = K_F C_e^{1/n} \quad (5)$$

where k_F is the Freundlich constant and n is the empirical constant.

Fig. 9 shows the modeling result and Table 3 lists corresponding parameters for the plots. By comparing the correlation coefficients (R^2) of the Langmuir model (R^2 = 0.965) and Freundlich model (R^2 = 0.986), the experimental values are suitable for both models especially the latter, demonstrating a favorable non-uniform adsorption condition on the heterogeneous surface. For the Langmuir isotherm model, the K_L (K_L = 0.024) was indicative of the binding propensity of fluoride ions unto Al–La hybrid adsorbent under the experiment conditions. Based on the Freundlich model, the value of $1/n$ was 0.496 within 0.1–1, also revealing the favorable of Al–La hybrid adsorbent in defluoridation. The maximum adsorption capacity could be analyzed as 28.383 mg g^{-1}. Moreover, the first inflection point in the curve was the result of competitive adsorption of fluoride ions between adsorbent and zinc ions in solution. Furthermore, the isotherm showed a trend almost perpendicular to the X axis in the dilute solution area, which should be attributed to capillary action appearing from the initial stage of adsorption.[35,36]

3.5. Synthesis and adsorption mechanisms

The FTIR spectra of the material are depicted in Fig. 10. According to the peaks between 400–800 in FTIR curve (a) and

Table 3 Langmuir and Freundlich adsorption isotherm parameters

Langmuir		Freundlich	
Parameter	Value	Parameter	Value
K_L	0.024	K_F	3.042
q_m	28.383	n	2.016
R^2	0.965	R^2	0.986

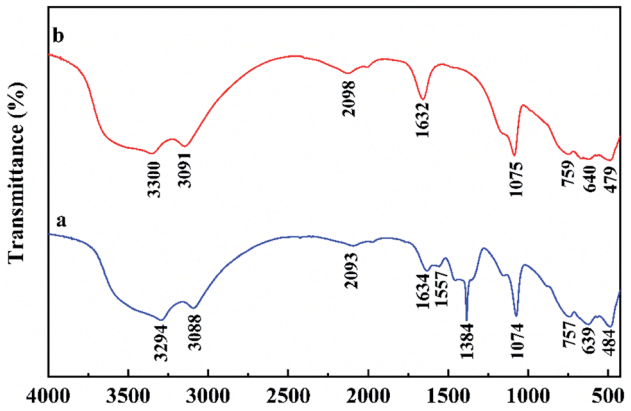

Fig. 10 FTIR spectra of the Al–La hybrid adsorbent before (a) and after (b) adsorption.

the crystalline state of lanthanum complex in TEM images, it can be inferred that lanthanum should exist in the form of lanthanum acetate. Hydrosol was obtained *via* mixing pseudo boehmite, lanthanum nitrate and acetic acid in deionized water under stirring. A large number of hydroxyl groups on the surface of the pseudo-boehmite crystallites adsorbed hydrogen ions as bridge to connect the hydroxyl groups of other pseudo-boehmite particles, which formed a network framework constituted by particles losing fluidity. Nitrate ions on the surface of the colloidal particles further constructed a stable electric double layer structure. Besides that, the generated lanthanum acetate entered the gaps of the network structure under the action of hydrogen bonding.

The simultaneous TG-DSC curves used to explore the further reaction of hydrogel in drying process are shown in the Fig. 11. The curves showed mass loss of the hydrogel from room temperature to 300 °C and thermal events corresponding to the loss. The fast mass loss accompanied by endothermic peak between 25 °C and 75 °C should be attributed to the removal of adsorbed water in hydrogel, whilst the slow mass loss step corresponding to the exothermic event between 75 and 170 °C was related to the continuous decomposition of nitric acid.

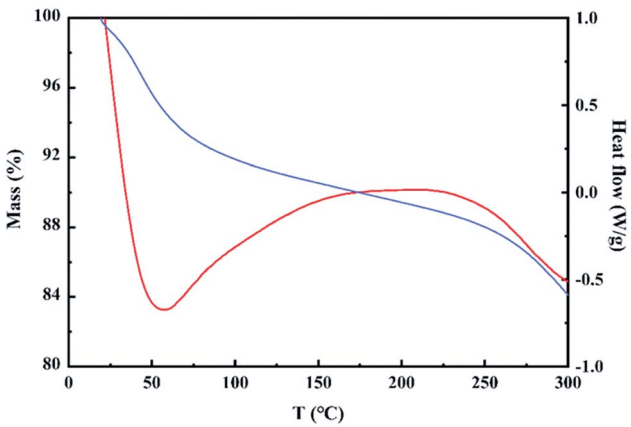

Fig. 11 TG-DSC curves of Al–La hydrogel.

Therefore, the changes in the drying process can be inferred as follows: The solid–liquid interface was gradually replaced by the solid–gas due to the evaporation of the adsorbed water, which produced the capillary action. A large amount of lanthanum acetate entered the aluminum intensive areas attributed to higher solid–liquid interfacial tension and stronger capillary action here. These small rings where aluminum gathered would not collapse attributed to the support of lanthanum acetate, and the interconnected mesopores conductive to defluoridation were formed.

TEM, BET and synthesis mechanism analyses revealed the mesoporous structure of synthesized materials. Based on the mesoporous structure and isotherm curve almost perpendicular to the *X* axis in the dilute solution area, it can be deduced that the adsorption process was accompanied by capillary action appearing from the initial adsorption stage. Therefore, in the initial adsorption stage, fluoride ions can not only be adsorbed by the protonated hydroxyl groups on the surface, but also be readily accessible to the protonated hydroxyl groups and rare earth ions in the pores through capillary action, producing the high fluoride ions adsorption rate with the removal rate reaching 50.88% within 1 min at 50 °C, 3 g L^{-1} (Fig. 7).

FTIR spectra (Fig. 10) of the Al–La hybrid adsorbent before and after adsorption were compared to further explore the adsorption mechanism.[37–39] The peak at 3294 cm^{-1} could be attributed to the tensile vibration of hydroxyl groups and the bands at 1634 cm^{-1} and 1557 cm^{-1} were assigned to the bending vibration of hydroxyl groups. These peaks were all shifted to higher wavelength positions in the composite after adsorption, which suggested that the hydroxyl groups adsorbed fluoride ions through electrostatic adsorption.[11] The adsorption bands between 400–800 cm^{-1} were derived from the presence of $La(CH_3COO)_3$. In the material after adsorption, the changes in peak shape indicated that lanthanum was complexed with fluoride ions.[18,19] Besides, the disappearance of the peak at 1384 cm^{-1} was due to the dissolution of nitrate ions in the sorbent during the adsorption process.

The element distribution of Al, La and F in the material after adsorption was investigated by EDS mapping method. As shown in Fig. 12, the element distribution of F and Al was similar, which indicated that the main mechanism of adsorption was the electrostatic adsorption of AlO(OH) to fluoride ions. It can be seen that La was mainly distributed in the gaps of AlO(OH), and a small amount of F was also present in the areas where La was dense. Therefore, it can be further confirmed that lanthanum had a complexing action on fluoride ions.

Based on the above analyses, the adsorption process mechanism can be inferred as follows: The Al–La hybrid adsorbent was a mesoporous material. The main body of this composite was γ-AlO(OH) with large area distribution, and $La(CH_3COO)_3$ was embedded in the AlO(OH). Compared with the rare earth modified aluminum-based materials prepared by traditional methods, the rare earth was loaded in the interior rather than on the surface of the aluminum matrix, forming a more stable structure. Many ink-bottle type mesopores were formed attributed to this distribution state. When in contact with zinc sulfate solution, the liquid quickly entered the pores through capillary

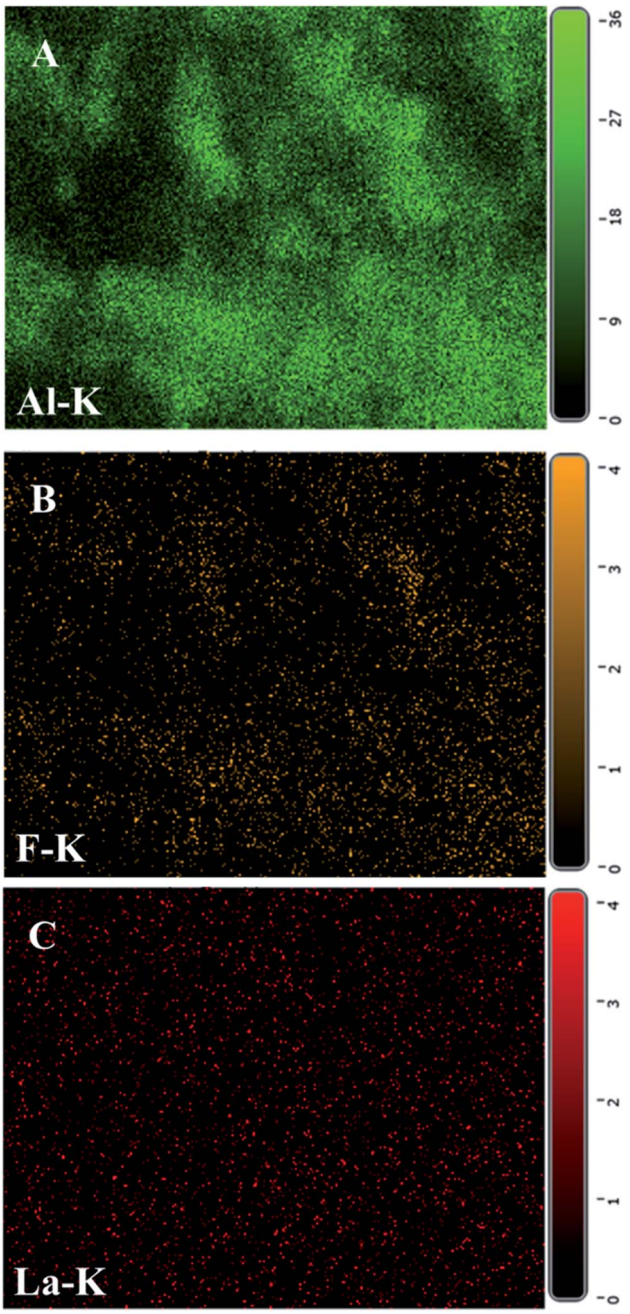

Fig. 12 EDS mapping of Al (A), F (B) and La (C) of the Al–La hybrid adsorbent after adsorption.

action. The fluoride ions in the solution were mainly adsorbed by the protonated hydroxyl groups through electrostatic adsorption, and a few fluoride ions were complexed by lanthanum.

4. Conclusions

Al–La hybrid gel was prepared by a simple sol–gel method innovatively and used for the adsorption of fluoride ions in zinc sulfate solution. The body of the sorbent was γ-AlO(OH) and $La(CH_3COO)_3$ was embedded in the host material, which formed large amounts of ink-bottle type mesopores. It could be found that at 50 °C, the adsorbent with amount of adsorbent of 3 g L^{-1} was able to get an excellent adsorption effect, and the adsorption equilibrium time after modification was shortened to 64 min under the influence of capillary effect. The pseudo-second-order kinetic model can fit the adsorption process well. The initial adsorption rate and the kinetic rate constant k_2 of Al–La hybrid gel were 11.372 mg g^{-1} min^{-1} and 0.06419 g min^{-1} g^{-1}, respectively (at temperature: 50 °C, initial fluoride ion concentration: 70.0 mg L^{-1}), showing an excellent kinetic performance compared with other aluminum-based adsorbents. For example, amorphous porous layered-Al_2O_3 derived from AlFu MOFs was used as an adsorbent for removing fluoride ions in industrial $ZnSO_4$ solution, the initial adsorption rate and the kinetic rate constant k_2 of it was 0.621 mg g^{-1} min^{-1} and 0.00633 g min^{-1} g^{-1}, respectively (at temperature: 40 °C, initial fluoride ion concentration: 120 mg L^{-1}).[9] The kinetic rate constant k_2 of a layered aluminum-based composite, which was used for adsorbing fluoride ions in industrial $ZnSO_4$ solution, was 0.03381 g min^{-1} g^{-1} (at temperature: 50 °C).[8] Additionally, the adsorption equilibrium time of Al–La hybrid was shortened to 64 min (at temperature: 50 °C, initial fluoride ion concentration: 70.0 mg L^{-1}), confirming the excellent kinetic performance compared with other aluminum-based adsorbents. As an example, the sorption equilibrium of an Al–Ce hybrid adsorbent was achieved within 5 h when the initial fluoride concentration was 5 g L^{-1}.[14] Both Langmuir model and Freundlich model matched the adsorption isotherm of the material well, and the adsorbent had a relative high sorption capacity up to 28.383 mg g^{-1} for fluoride, higher than that of some aluminum based adsorbent adsorbents (*e.g.* The maximum adsorption capacity of a La^{3+}-modified activated alumina for fluoride removal was 6.70 mg g^{-1}.[12]). It can be concluded that the adsorption should be a process based on the electrostatic adsorption of hydroxy and lanthanum fluoride complexation, and accompanied by capillary action existed from the initial stage of adsorption. In conclusion, since both AlO(OH) and $La(CH_3COO)_3$ had a large number of fluoride ion adsorption sites, the Al–La hybrid gel possessed an ideal adsorption capacity. In addition, the adsorption rate was greatly enhanced by the filling load mode of the composite. The stable structure and the synthetic method with low time and energy consumption also revealed a large difference of Al–La hybrid gel from other aluminum-based adsorbents. Although the selectivity for fluoride ion needs to be improved, Al–La hybrid adsorbent suggests potential applications in defluoridation from zinc sulfate electrolytes as well as other solutions with complicated composition and ions form.

Conflicts of interest

There are no conflicts to declare.

Acknowledgements

This work was supported by the Key Laboratory Project of Shaanxi Provincial Department of Education (No. Z202001511)

and the Punai Functional Materials Co., Ltd (Contract No. 20200216).

Notes and references

1 A. Banihashemi, K. Zare, V. Javanbakht and H. Mohammadifard, *Mater. Chem. Phys.*, 2021, **258**, 123934.
2 A. Jeyaseelan, M. Naushad, T. Ahamad and N. Viswanathan, *J. Environ. Chem. Eng.*, 2020, 104563.
3 N. Antuñano, J. F. Cambra and P. L. Arias, *Hydrometallurgy*, 2016, **161**, 65–70.
4 S. Mandal and S. Mayadevi, *Chemosphere*, 2008, **72**, 995–998.
5 Q. Zhang and Y. Hua, *Mater. Chem. Phys.*, 2012, **134**, 333–339.
6 S. Tokunaga, M. J. Haron, S. A. Wasay, K. F. Wong, K. Laosangthum and A. Uchiumi, *Int. J. Environ. Stud.*, 1995, **48**, 17–28.
7 X. Wu, Z. Liu and X. Liu, *Hydrometallurgy*, 2014, **141**, 31–35.
8 Z. Tian, W. Guo, Z. Zhang, Y. Lai, S. Ye and J. Li, *Hydrometallurgy*, 2017, **171**, 222–227.
9 K. Yang, Y. Li, Z. Zhao, Z. Tian and Y. Lai, *Chem. Eng. Res. Des.*, 2020, **153**, 562–571.
10 P. Loganathan, S. Vigneswaran, J. Kandasamy and R. Naidu, *J. Hazard. Mater.*, 2013, **248–249**, 1–19.
11 S. Deng, H. Liu, W. Zhou, J. Huang and G. Yu, *J. Hazard. Mater.*, 2011, **186**, 1360–1366.
12 J. Cheng, X. Meng, C. Jing and J. Hao, *J. Hazard. Mater.*, 2014, **278**, 343–349.
13 S. Jagtap, M. K. Yenkie, N. Labhsetwar and S. Rayalu, *Chem. Rev.*, 2012, **112**, 2454–2466.
14 H. Liu, S. Deng, Z. Li, G. Yu and J. Huang, *J. Hazard. Mater.*, 2010, **179**, 424–430.
15 S. Tokunaga, M. J. Haron, S. A. Wasay, K. F. Wong, K. Laosangthum and A. Uchiumi, *Int. J. Environ. Stud.*, 1995, **48**, 17–28.
16 A. Ghosh, S. Chakrabarti, K. Biswas and U. C. Ghosh, *Appl. Surf. Sci.*, 2014, **307**, 665–676.
17 A. M. Raichur and M. Jyoti Basu, *Purif. Technol.*, 2001, **24**, 121–127.
18 Y. He, L. Zhang, X. An, G. Wan, W. Zhu and Y. Luo, *Sci. Total Environ.*, 2019, **688**, 184–198.
19 X. Wei, G. Zhang, Y. Zhang, D. Tang and J. Wang, *Chem. Eng. J.*, 2014, **250**, 423–430.
20 S. W. K. Sing, *Pure Appl. Chem.*, 1985, **57**, 603–619.
21 D. Dayananda, V. R. Sarva, S. V. Prasad, J. Arunachalam and N. N. Ghosh, *Chem. Eng. J.*, 2014, **248**, 430–439.
22 E. C. Nnadozie and P. A. Ajibade, *Microporous Mesoporous Mater.*, 2020, **309**, 110573.
23 M. Li, D. Wei, T. Liu, Y. Liu, L. Yan, Q. Wei, B. Du and W. Xu, *Sep. Purif. Technol.*, 2019, **227**, 115696.
24 Y. S. Ho and G. McKay, *Process Biochem.*, 1999, **34**, 451–465.
25 G. E. J. Poinern, M. K. Ghosh, Y.-J. Ng, T. B. Issa, S. Anand and P. Singh, *J. Hazard. Mater.*, 2011, **185**, 29–37.
26 N. Chen, Z. Zhang, C. Feng, M. Li, D. Zhu, R. Chen and N. Sugiura, *J. Hazard. Mater.*, 2010, **183**, 460–465.
27 X. Fan, D. J. Parker and M. D. Smith, *Water Res.*, 2003, **37**, 4929–4937.
28 Y. S. Ho, *J. Hazard. Mater.*, 2006, **136**, 681–689.
29 A. Mittal, L. Kurup and J. Mittal, *J. Hazard. Mater.*, 2007, **146**, 243–248.
30 G. Sugihara, D. S. Shigematsu, S. Nagadome, S. Lee, Y. Sasaki and H. Igimi, *Langmuir*, 2000, **16**, 1825–1833.
31 K. Y. Foo and B. H. Hameed, *Chem. Eng. J.*, 2010, **156**, 2–10.
32 F. Gimbert, N. Morin-Crini, F. Renault, P.-M. Badot and G. Crini, *J. Hazard. Mater.*, 2008, **157**, 34–46.
33 Y. Liu, H. Xu and J.-H. Tay, *J. Environ. Eng.*, 2005, **131**, 1466–1468.
34 C. K. Aslani and O. Amik, *Appl. Radiat. Isot.*, 2020, 109474.
35 J. Van Brakel and P. M. Heertjes, *Nature*, 1977, **268**, 44–45.
36 G. Reichenauer and G. W. Scherer, *Colloids Surf., A*, 2001, **187–188**, 41–50.
37 L. Li, H. Ren, Y. Liu, X. Liu, Y. Zhao, X. Zhou, W. Kang, X. Zhuang and B. Cheng, *Microporous Mesoporous Mater.*, 2020, **308**, 110544.
38 E. Santoso, R. Ediati, Z. Istiqomah, D. O. Sulistiono, R. E. Nugraha, Y. Kusumawati, H. Bahruji and D. Prasetyoko, *Microporous Mesoporous Mater.*, 2021, **310**, 110620.
39 R. Yu and Z. Wu, *Microporous Mesoporous Mater.*, 2020, **308**, 110494.